NANO LETTERS

2008
Vol. 8, No. 1
221−226

Herding Nanotransporters: Localized Activation via Release and Sequestration of Control Molecules

Robert Tucker, Parag Katira, and Henry Hess*

Department of Materials Science and Engineering, University of Florida, Gainesville, Florida 32611-6400

Received October 1, 2007; Revised Manuscript Received November 21, 2007

ABSTRACT

A challenge for nanotechnology is the dynamic and specific control of nanomachines by the user. Molecular shuttles, consisting of cargo-binding microtubules propelled by surface-immobilized kinesin motor proteins, are an example of a nanoscale system that ideally can be selectively activated at programmable locations and times. Here we discuss a biomimetic solution where activating molecules are delivered locally via photolysis of a caged compound and subsequently sequestered in an enzymatic network. The controlled sequestration of the activator not only creates a rapid deactivation when the stimulus is removed but also sharpens the concentration profile of the rapidly diffusing activator. This improvement comes at the expense of a reduced efficiency in the utilization of the activator molecules, suggesting that these nanosystems are most efficiently addressed as a swarm rather than as individuals. Our work represents a step toward transferring the cellular control strategies of molecular activation to bionanotechnology.

Bionanotechnology is concerned with the utilization of biological components in nanotechnology,[1] which to a varying degree necessitates the use of biological engineering approaches in a wider sense, for example, in the use of self-assembly to create extended structures. However, a striking accomplishment of nature is not only to create nanomachines and weave them into larger structures, but also to control their spatial and temporal activation via specific signals. This controlled activation is often achieved through the delivery of small molecules, whose spatial and temporal distribution is shaped by the actions of multiple enzymes releasing or sequestering the activating species. Examples include intracellular signaling via calcium,[2,3] NAD(P)H,[4] or cAMP.[5]

In contrast, the dynamic and controlled activation of specific nanomachines has been addressed in a technological context primarily by making light-activation an integral part of the design as in the light-driven synthetic motors based on rotaxanes or catenanes[6] or by designing devices that can be individually activated with a highly specific fuel molecule.[7] A new, chemical approach is to exploit reaction-diffusion systems to locally change buffer conditions and activate enzymes.[8]

Here, we present a biomimetic approach to dynamically control motor protein-driven bionanodevices[9] in particular kinesin-driven molecular shuttles.[10] Molecular shuttles consist of a surface patterned with stationary kinesin motors and cargo-binding microtubules transported by the motors. Localized release and enzymatic sequestration of the substrate ATP creates a spatially and temporally well-defined concentration profile, which in turn leads to controlled activation of a small number of molecular shuttles, as shown in Figure 1. This approach significantly expands the scope of previous work,[11] which demonstrated that repeated, stepwise activation of kinesin-driven molecular shuttles can be achieved by

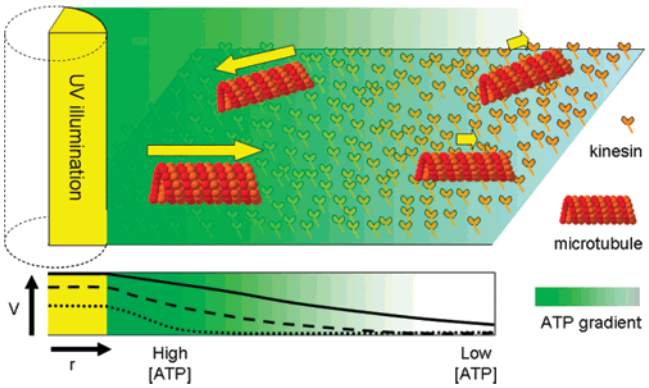

Figure 1. Light activation and control of molecular shuttles. A nearly cylindrical cone of UV light is produced within a flowcell to locally photolyze caged-ATP. As the ATP diffuses outward, it is hydrolyzed by kinesin, resulting in localized microtubule movement. Hexokinase is added to the solution to increase the gradient of the ATP concentration profile. As the hexokinase concentration is increased, the area of activation and the maximum shuttle speed decrease.

* Corresponding author. Fax: (352) 846-3355. Tel: (352) 846-3781. E-mail: hhess@mse.ufl.edu.

10.1021/nl072516n CCC: $40.75
Published on Web 12/15/2007

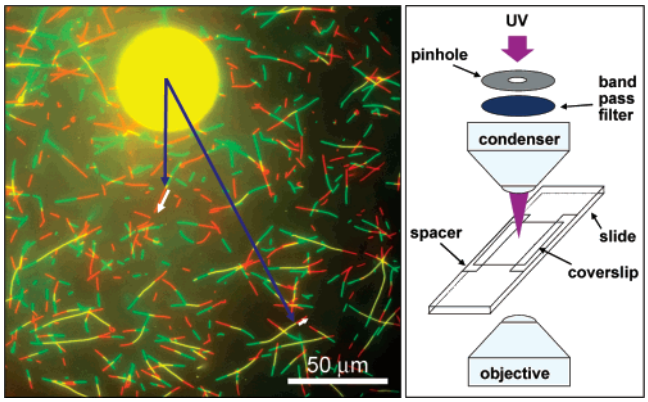

Figure 2. Measurement of shuttle velocity and radial distance from the center of illumination and the experimental setup. Left: Two images (pseudocolored in green and red and separated by 200 s in time) are overlaid, showing the illumination zone and the movement of microtubules with radius-dependent velocity, due to the ATP sequestration by hexokinase in solution (50 units/L). Right: The experimental setup.

photolysis of caged-ATP in a solution of hexokinase without localization and on the time scale of minutes.

The necessity for this basic enzymatic network arises from the rapid diffusion of ATP ($D = 3 \times 10^{-10}$ m^2/s),[12] which outpaces the movement of kinesin-driven molecular shuttles by a factor of 100 on the time scale of 1 s (or 10 on the time scale of one motor step). The presence of hexokinase in the solution limits the average distance an ATP molecule can diffuse and leads to an increased spatial gradient of the kinesin activity.

The localization of the illumination with UV light and thus the photolysis of caged-ATP to a cylindrical region with a radius of either 15 or 25 μm leads to a dramatic improvement in the temporal control over the shuttle activation. The shuttles immediately (<1 s) respond to the illumination by beginning to move. After the illumination ends, the shuttle velocity drops by 1/e on a time scale of 10 s without sequestration by hexokinase to 1 s with hexokinase present (Supporting Information, Figure 1). Previously,[11] uniform illumination of the cell led to deactivation on a time scale of hours to minutes in the absence and presence of hexokinase, respectively. Of course, this improved temporal control is a consequence of the rapid diffusion of the released ATP away from the illumination zone and its dilution in the surrounding solution.

Repeated illumination with 250 ms pulses causes the shuttles to move a distance equal to the distance traveled with a single pulse equal to the total duration of illumination (Supporting Information, Figure 2), which implies that the average translation per pulse can be tuned to less than 50 nm.

While the diffusion of the activating molecule, ATP, benefits the control of activation in the temporal domain, the situation is reversed in the spatial domain.

We measured the velocity of individual shuttles as function of their distance from the center of illumination (Figure 2) to determine velocity profiles. Because the velocity profiles of pulsed and continuous illumination were very similar

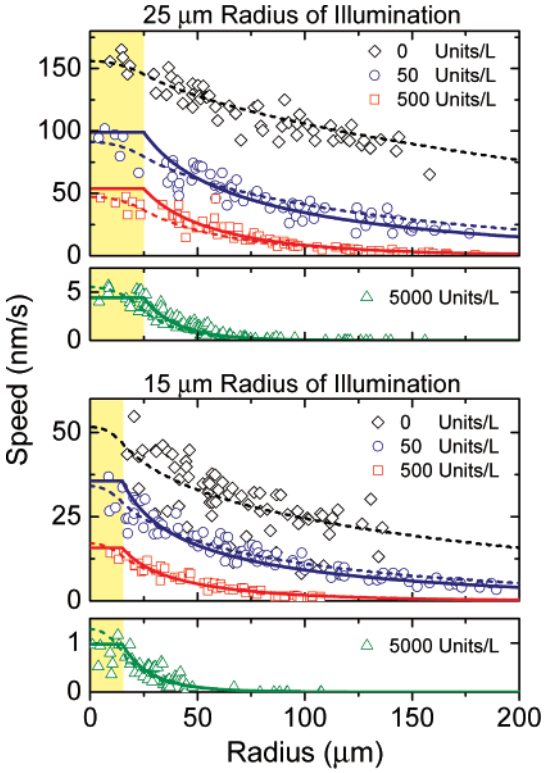

Figure 3. Velocity profiles. Velocities of individual shuttles are measured as a function of the distance from the center of illumination for illumination zones with a radius of 25 and 15 μm at different hexokinase concentrations (0, 50, 500, 5000 units/L). Dashed lines are the numerical solutions and solid lines are the analytical solutions as described in the text.

(Supporting Information, Figure 2), the discussion will focus on the steady-state between the release, diffusion, and sequestration of ATP reached during extended illumination. The velocity profiles correspond closely to ATP concentration profiles, because shuttle velocities were less than 20% of the maximum velocity at saturating ATP concentrations.

The velocity profiles (Figure 3) show an approximately exponential decay of the velocity with increasing radius. As the hexokinase concentration in the solution is increased from 0 to 5000 units/L, the accelerated sequestration of ATP leads to a reduction of shuttle velocity by a factor of 30−50 and a sharpening of the concentration profile by a factor of 5−7. Changing the radius of the illumination zone from 25 to 15 μm reduces the observed velocities to a third, roughly in proportion to the area of the illumination zone (at constant light intensity).

To model the system, the diffusion equation was augmented with a generation term describing the release of ATP (as a function of light intensity and size of illumination zone) and a sequestration term describing the consumption of ATP by hexokinase and solved numerically for cylindrical symmetry (see Materials and Methods). A velocity profile was calculated from the generated time-dependent ATP concentration profile using the Michaelis−Menten equation for kinesin with $K_m = 25$ μM and $v_{max} = 1000$ nm/s.[13−15] In the presence of hexokinase, continuous illumination led to a steady state in less than 500 s. In the absence of hexokinase, the width of the velocity profile increases with the third root

of the illumination time and reaches 0.2 mm full width at half maximum (FWHM) after 200 s.

However, to obtain a good fit to the experimental data, the calculated velocity profile (at the time of observation) had to be multiplied by a factor *f*, ranging from 1 for the curve with the highest observed velocity (150 nm/s) to 0.05 for the curve with the lowest observed velocity (1 nm/s). This is likely a result of slowing interactions between the multiple kinesin motors transporting each microtubule at small ATP concentrations, an effect that has been previously experimentally observed[13] and is also suggested by theoretical considerations.[16]

The excellent fit between the shape of the calculated and the measured velocity profile proves that the model approximations (e.g., neglecting the hydrolysis of ATP by the kinesin motors and the depletion of caged-ATP in the illumination zone) are justified.

Additional insights into the process are obtained from analytically solving the steady-state reaction diffusion equation with cylindrical symmetry outside the illumination zone. In the present situation, a characteristic diffusion distance r^* can be defined for the ATP molecules by $r^{*2} = (K_m D/A)$ where $D = 300\ \mu m^2/s$ is the diffusivity of ATP, $K_m = 0.12$ mM is the Michaelis constant of hexokinase with respect to ATP, and A is the activity of the hexokinase solution. The approximate solution[17] of the reaction diffusion equation outside the illumination zone can be written in terms of r^* and the radius of the illumination zone r_i as (detailed calculations in the Supporting Information)

$$C = C_0\sqrt{\frac{r_i}{r}}\cdot\exp\left[\frac{(r_i - r)}{r^*}\right] \qquad (1)$$

where C_0 is the ATP concentration at the boundary of the illuminated zone.

Velocity profiles (Figure 3) are calculated from eq 1 using $v = fv_{max}C/K_m^{kin}$, where f is the above-mentioned factor accounting for slowing motor interactions, K_m^{kin} is the Michaelis constant for ATP consumption by kinesin, and small ATP concentrations are assumed.

The experimental data are fit to the above expression for v outside the illumination zone while the velocity within the zone is assumed to be constant and equal to $v_0 = fv_{max}C_0/K_m^{kin}$. The fit to the six experimental profiles utilizes six values of C_0 as free parameters while the value of r^* is obtained from the known values of K_m, D, and A ($r^* = 210$, 66, and 21 μm for 50, 500, and 5000 units/L of hexokinase, respectively), and the values of f are the same as in the numerical simulations. The values of C_0 obtained from the fits are 1.4, 0.9, 0.5 μM for $r_i = 15\ \mu$m at 50, 500, and 5000 units/L hexokinase activity and 3.3, 1.9, 0.7 μM for $r_i = 25$ μm at 50, 500, and 5000 units/L hexokinase activity, respectively.

By equating the rate of ATP consumption integrated over all radii with the rate G of ATP generation from caged-ATP, the ATP concentration C_0 in the illumination zone and at the boundary can be determined (see Supporting Information). At low light intensities, the ATP generation is not limited by the diffusive influx of caged ATP into the illumination region but is given by $G = C_{cATP} \times k \times I_{h\nu}$, where C_{cATP} is the constant concentration of caged-ATP, k is the ATP uncaging rate constant and $I_{h\nu}$ is the UV light intensity.[18] Thus

$$C_0 = \frac{C_{cATP}kI_{h\nu}}{D\left(\frac{1}{r^*} + \frac{1}{r_i}\right)^2} \qquad (2)$$

On the basis of the known values for C_{cATP}, D, r^*, r_i, k, and the fit values for C_0, this implies that the average illuminating UV intensity is 2 mW/cm^2 for both pinhole sizes.

The analytical solution illustrates the opposing trends in achieving localized control: A reduction in the characteristic ATP diffusion distance r^* (increase in hexokinase activity) leads to reduced ATP levels (Figure 4A) but at the same time narrows the ATP plume as measured by the radius at which the shuttle velocity is reduced to 10% of the maximum ($r_{10\%}$, Figure 4B). Interestingly, if the absolute concentration gradient $C_0/r_{10\%}$ is used as the performance metric of the control process (Figure 4C), it becomes apparent that an optimum for the characteristic diffusion distance exists.

Because $r_{10\%} \approx r_i + r^*$ for $r^* < 10r_i$ (Figure 4B), by finding the maximum of $C_0/(r_i + r^*)$ the optimal value of the characteristic diffusion distance r^* can be determined to be approximately equal to twice the illumination radius r_i (Figure 4C and Supporting Information).

This suggests a strategy to achieve a desired level of control in the case of cylindrical symmetry: (1) Define the size of the activation zone given by $r_{10\%}$, (2) restrict illumination to a third of the activation zone $r_i = r_{10\%}/3$, (3) adjust the activity of the sequestration enzyme so that the characteristic diffusion distance equals twice the radius of the illumination zone ($r^* = 2r_i$), and (4) tune the concentration of caged-ATP and the intensity of illumination to achieve the desired speed within the illumination zone.

Unfortunately, even in the optimal case a decrease in the size of the activation zone leads to a linear decrease of the generated gradient and a quadratic decrease in fuel efficiency, which is defined here as the ratio of the number ATP molecules used by motors to the total number of ATP molecules released. The decreasing gradient can be compensated by increasing the intensity of the light source, but the amount of ATP that can be released is ultimately limited by the influx of caged-ATP into the illumination zone. However, the light intensity at this limit is expected to lead to unacceptable levels of photodamage (see Supporting Information for detailed discussion).

The above-described experiments, simulations, and calculations demonstrate a significant improvement in the control of molecular shuttles. However, they also point out a tradeoff: while the sequestration of small molecules that govern the activation of nanosystems improves the spatial and temporal control, even a restriction of the activation zone to tens of micrometers reduces the activation level drastically. At the same time, the vast majority of the released control

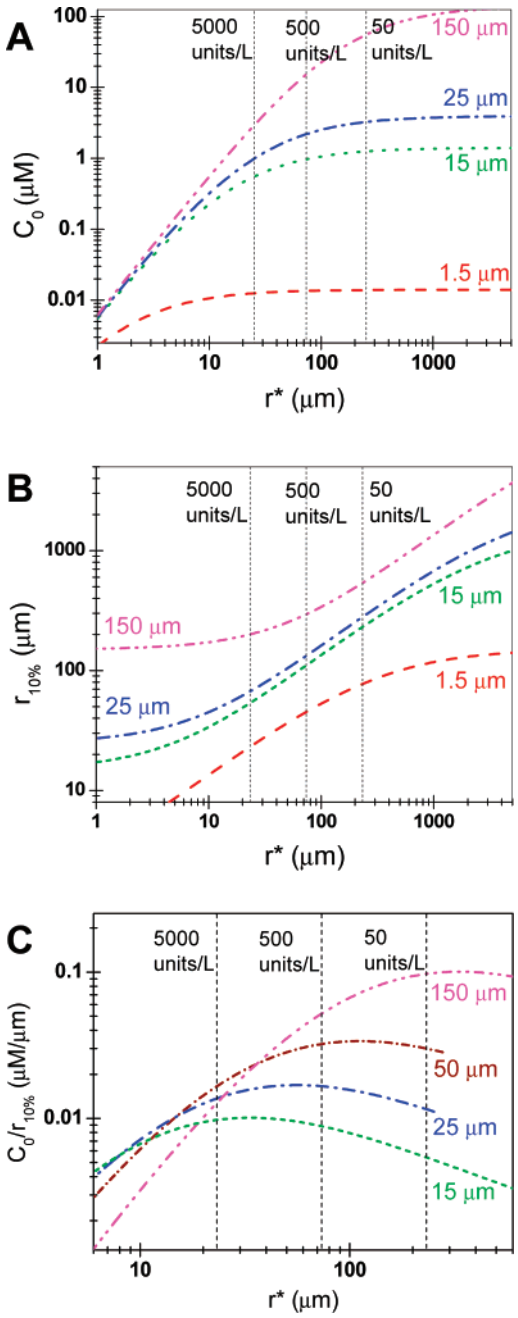

Figure 4. Relationships between the maximum ATP concentration (A), the distance at which the ATP concentration drops to 10% of its maximum (B), and the control performance (C) and the characteristic distance according to eqs 1 and 2. The broken vertical lines indicate the hexokinase activities used in the experiments with illumination zones of radius 15 and 25 μm.

molecules do not even interact with the nanomachines. These general considerations apply in a variety of experimental situations. For example, small molecules may be delivered by injection into a fluid stream that rapidly removes them from a stationary target.[19] Metal ions may control the activation of a restriction enzyme[8] or F1-ATPase[20] and be sequestered by a chelator, and DNA motors[21,22] are controlled by DNA oligomers that may in turn be removed by other oligomers. In the context of molecular shuttles, the release of cargo can be achieved by delivering a competitor for the cargo linkage.[23,24]

Alternatives to control via activating molecules exist but are not superior. Localized heating in a cold environment[25,26] has been demonstrated; however, for kinesin motors a 10-fold difference in activation (chosen here as benchmark to define the activation zone) is difficult to achieve due to the limited range of protein stability.[27] Similarly, optical molecular switches can overcome diffusion limitations, but currently only a roughly 5-fold difference in activity between the on- and off-state of the controlled nanosystem has been demonstrated.[28,29] Electronic switching of enzyme activity is promising, if the currently achieved on/off ratio of 3/2 can be improved.[30] Control by uncaging and sequestration of control molecules in contrast could potentially be increased up to the diffusion limit (eq 11, Supporting Information) by employing a more brilliant light source (e.g., a UV laser) and minimizing photodamage. A complementary approach to control is "steering", where fluid flow, electric, and magnetic fields are applied to orient actin filaments or microtubules.[31−36] In this case, motor activity is not targeted. Similarly, switching the properties of a surface to promote/inhibit the ability of adhered motors to bind microtubules controls microtubule density rather than motor activation.[37]

Our findings reiterate that due to the rapid diffusion of information in integrated molecular factories, as exemplified by cells, spatial organization of the workflow is not efficient in contrast to the macroscale. Instead, information has to be stored in and manipulated between a multitude of different chemical species. While we show that activation can be successfully constrained by local release and rapid sequestration, it may be more natural to employ molecular shuttles as parts of a large and dispersed swarm rather than individually. To quote Hofstadter's anteater, "... you must not take an ant for the colony".[38] The engineering task is then to tailor the swarm behavior, for example, by limiting dispersion[39] or by self-generating ATP[40] rather than the individual nanotransporter.

The insights generated from this investigation of control via diffusing molecules may also inform work at the interface of BioNEMS and systems biology,[41] in molecular computing,[42] and in the emerging field of bio-nanologistics.[43]

Materials and Methods. *Kinesin and Microtubules.* Full length, wild-type kinesin from *Drosophila melanogaster* expressed with a C-terminal histidine-tag in *E. coli* was purified using a Ni-NTA column as described in ref 44. Microtubules were polymerized as follows: Polymerization buffer (80 mM Pipes, 1 mM EGTA, 5 mM $MgCl_2$, 1 mM guanosine 5′-triphosphate, and 5% dimethylsulfoxide) was added to a 20 μg aliquot of rhodamine-labeled tubulin (TL331M, Cytoskeleton, Denver, CO) resulting in a final tubulin concentration of 32 μM. The solution was kept at 37 °C for 30 min and then diluted 100-fold in BRB80 (80 mM PIPES, 1 mM MgCl, 1 mM EGTA, pH 6.9) containing 10 μM taxol for stabilization and kept at room temperature (20 °C).

Caged-ATP and Hexokinase. Photocleavable 1-(4,5-dimethoxy-2-nitrophenyl)ethyl-caged-ATP (Molecular Probes, Eugene, Oregon) was dissolved in nanopure H_2O to a final concentration of 10 mM.

Hexokinase (H-5625, Sigma-Aldrich, St. Louis, MO) was dissolved in BRB80 to create stock solutions of 1000−400 000 units/L. These stock solutions were then diluted in motility solutions resulting to final concentrations of 25−5000 units/L. The K_M for hexokinase with respect to ATP is 120 μM.[45]

Motility Assays and Microscopy. The motility assays were performed in 100 μm high, 1.5 cm wide flowcells.[46] Casein (0.5 mg/mL, Sigma-Aldrich, St. Louis, MO) dissolved in BRB80 was adsorbed for 5 min to reduce denaturation of kinesin. Kinesin (10 nM kinesin, 1 mM MgATP, 0.5 mg/mL casein, BRB80) was then adsorbed for 5 min. Finally, the motility solution containing the caged ATP was flowed into the flowcell (32 nM microtubules, 500 μM caged-ATP, and an oxygen-scavenging system consisting of 20 mM D-glucose, 0.02 mg/mL glucose oxidase, 8 μg/mL catalase, 1% dithiotreitol in BRB80). D-glucose is simultaneously the substrate for glucose oxidase and hexokinase. Hexokinase hydrolyzes ATP while phosphorylating D-Glucose, producing ADP and glucose-6-phosphate. Because the K_M of hexokinase for glucose is 120 μM, the hexokinase activity is limited only by the ATP concentration.

The flowcells were imaged using an epifluorescence microscope (Eclipse TE2000U, Nikon) with a 100 W Hg lamp, a 40× oil objective (NA 1.4), a cooled CCD camera (Andor iXon, Andor Technology, Windsor, CT), and a rhodamine filter set (Filter Set 48002, Chroma Technology Corp, Rockingham, VT). The ultraviolet illumination in the wavelength range from 325 to 375 nm was provided by a xenon arc lamp (Lambda-LS, Sutter Instrument, Novato, CA) with a liquid-light guide and passed through circular pinhole with a radius of 150 or 250 μm (Edmund Optics Inc.) and a UV filter (Chroma D350/50x, Chroma Technology Corp, Rockingham, VT). A 10× demagnified image of the pinhole was projected by the condenser (High N.A. Condenser, Nikon Instruments) to the object plane of the microscope. The aperture stop of the condenser was almost completely closed to create a nearly cylindrical light path (Figure 1) with a conical angle of 6°.

The light passing through the flowcell was measured using a hand-held power meter (model 3803, New Focus, San Jose, CA) calibrated with a UV-sensing power meter (Mannix UV-340 Light Meter, Ambient Weather, Tempe, AZ). Within the flowcell, this light power of 0.8 and 1.3 μW was focused into a near cylindrical cone with a radius of 15 and 25 μm resulting in an intensity of 110 and 65 mW/cm^2, respectively. These intensities are 50-fold higher than the intensity implied from the analytical and numerical fits to the data. We were unable to resolve this discrepancy.

All assays were performed at 20 °C.

Velocity and Radius Measurements. The image acquisition settings were chosen according to the velocity of the shuttles. The time between image acquisitions for both pinholes was 10, 10, 40, and 80 s for hexokinase activities of 0, 50, 500, and 5000 units/L, respectively. The exposure time for all images was 500 ms.

For steady-state experiments, the UV source was "on" continuously throughout the experiment and velocity measurements were begun after a minimum of 100 s of UV illumination and extended up to 1000 s. The radial distance was measured from the center of the pinhole to the leading edge of the microtubule in the initial image (blue arrow, Figure 2). The velocity is given by the ratio of the distance between the leading edge of the microtubule in the two images (white arrow) divided by the time between images (200 s in Figure 2). Images were skipped to increase the accuracy at low velocities.

For the pulsing experiments, the UV source was on for 250 ms and off for 1750 ms, for a total cycle time of 2 s. One thousand pulsing cycles were performed for each hexokinase concentration and pinhole, and the velocity and radius measurements were then derived from these images. The shuttle velocity was calculated by dividing the distance traveled by the on time.

Numerical Model. The following second-order partial differential equation in cylindrical symmetry was solved for the ATP concentration within the flowcell using the ODE-solve routine in MathCAD 13.1 (Parametric Technology Corp., Needham, MA):

$$\frac{\partial^2[\mathrm{ATP}]}{\partial t^2} = \mathrm{D}\frac{\partial^2[\mathrm{ATP}]}{\partial r^2} + \frac{D}{r}\cdot\frac{\partial[\mathrm{ATP}]}{\partial r} + G(r,t) - A\frac{[\mathrm{ATP}]}{K_m + [\mathrm{ATP}]} \quad (3)$$

Here, the ATP concentration depends on the radial diffusion of the ATP (first two terms), the ATP generated within the pinhole (third term), and sequestration by hexokinase (fourth term). The ATP concentration is assumed to be zero initially and at a 1 mm distance from the center of the flowcell for all times. The K_m for hexokinase was set to 120 μM.[45] The measured light intensity was used to calculate a first ATP uncaging rate $G(r,t)$ within the cylindrical illumination zone using previously determined photolysis rates.[18] The uncaging rate was then tuned to fit the experimental data shown in Figure 3.

The resulting ATP concentration profile was then used to calculate the molecular shuttle velocity assuming Michaelis−Menten kinetics of kinesin with a v_{max} of 1000 nm/s, a K_m^{kin} of 25 μM, inhibition constants (K_i) for ADP and caged-ATP of 35 and 200 μM[18]

$$V = f\frac{[\mathrm{ATP}]}{[\mathrm{ATP}] + K_m^{kin} + [\text{caged-ATP}]\frac{K_m^{kin}}{K_i^{\text{caged}-\mathrm{ATP}}} + [\mathrm{ADP}]\frac{K_m^{kin}}{K_i^{ADP}}} \quad (4)$$

The factor f accounts for the decreasing shuttle velocity at small ATP concentrations and was chosen as 0.75, 0.7, 0.6, 0.4, 0.15, and 0.05 for shuttle velocities at the center of illumination of 65−100, 60, 40, 20, 6, and 1 nm/s, respectively. The time to reach steady-state for constant UV illumi-

nation varied depending on the pinhole size and hexokinase concentration, but steady state was always reached within 500 s.

Acknowledgment. We thank Viola Vogel for her support during the initial stages of the project, Stefan Diez for fruitful discussions, and Ashutosh Agarwal for programming the image acquisition software. R.T. thanks the Fulbright Program for a graduate fellowship. Financial support was provided by the DARPA Biomolecular Motors program (AFOSR FA 9550-05-1-0366) and NSF (DMR 0645023). R.T. conducted the experiments and the numerical modeling, P.K. contributed the analytical modeling, and H.H. coordinated the research.

Supporting Information Available: Supplementary calculations for the analytical solution of the reaction/diffusion problem, the fuel efficiency, and the diffusion-limited uncaging of ATP at high light intensities. Figures illustrate exponential decay of modeled and experimental stoppage time and the comparison of constant and pulsed illumination. Movies depict diffusion-limited control and enzymatic control. This material is available free of charge via the Internet at http://pubs.acs.org.

References

(1) Niemeyer, C. M.; Mirkin, C. A. *Nanobiotechnology*; Wiley-VCH: Weinheim, 2004; p 469.
(2) Alkon, D. L.; Rasmussen, H. *Science* **1988**, *239* (4843), 998−1005.
(3) Berridge, M. J.; Bootman, M. D.; Roderick, H. L. *Nat. Rev. Mol. Cell Biol.* **2003**, *4* (7), 517−529.
(4) Kindzelskii, A. L.; Petty, H. R. *Proc. Natl. Acad. Sci. U.S.A.* **2002**, *99* (14), 9207−9212.
(5) Alberts, B.; Johnson, A.; Lewis, J.; Raff, M.; Roberts, K.; Walter, P. *Molecular Biology of the Cell*, 4th ed.; Garland: New York, 2002.
(6) Balzani, V. V.; Credi, A.; Raymo, F. M.; Stoddart, J. F. *Angew. Chem., Int. Ed.* **2000**, *39* (19), 3348−3391.
(7) Yan, H.; Zhang, X.; Shen, Z.; Seeman, N. C. *Nature* **2002**, *415* (6867), 62−5.
(8) Namasivayam, V.; Larson, R. G.; Burke, D. T.; Burns, M. A. *Anal. Chem.* **2003**, *75* (16), 4188−4194.
(9) Hess, H.; Bachand, G. D.; Vogel, V. *Chem.—Eur. J.* **2004**, *10* (9), 2110−2116.
(10) Hess, H.; Vogel, V. *Rev. Mol. Biotechnol.* **2001**, *82* (1), 67−85.
(11) Hess, H.; Clemmens, J.; Qin, D.; Howard, J.; Vogel, V. *Nano Lett.* **2001**, *1* (5), 235−239.
(12) de Graaf, R. A.; van Kranenburg, A.; Nicolay, K. *Biophys. J.* **2000**, *78* (4), 1657−1664.
(13) Howard, J.; Hudspeth, A. J.; Vale, R. D. *Nature* **1989**, *342*, 154−158.
(14) Schief, W. R.; Clark, R. H.; Crevenna, A. H.; Howard, J. *Proc. Natl. Acad. Sci. U.S.A.* **2004**, *101* (5), 1183−8.
(15) Saha, A. K.; Katira, P.; Hess, H. *Small*, submitted for publication, 2007.
(16) Klumpp, S.; Lipowsky, R. *Proc. Natl. Acad. Sci. U.S.A.* **2005**, *102* (48), 17284−9.
(17) Bronshtein, I. N.; Semendyayev, K. A.; Musiol, G.; Muehlig, H., *Handbook of Mathematics*, 4th ed.; Springer: Berlin, 2004.
(18) Wu, D.; Tucker, R.; Hess, H. *IEEE Trans. Adv. Packag.* **2005**, *28* (4), 594−599.
(19) Beta, C.; Wyatt, D.; Rappel, W. J.; Bodenschatz, E. *Anal. Chem.* **2007**, *79*, (10), 3940−3944.
(20) Liu, H.; Schmidt, J. J.; Bachand, G. D.; Rizk, S. S.; Looger, L. L.; Hellinga, H. W.; Montemagno, C. D. *Nat. Mater.* **2002**, *1* (3), 173−177.
(21) Yurke, B.; Turberfield, A. J.; Mills, A. P.; Simmel, F. C.; Neumann, J. L. *Nature* **2000**, *406* (6796), 605−608.
(22) Bath, J.; Turberfield, A. J. *Nat. Nanotechnol.* **2007**, *2* (5), 275−284.
(23) Hirabayashi, M.; Taira, S.; Kobayashi, S.; Konishi, K.; Katoh, K.; Hiratsuka, Y.; Kodaka, M.; Uyeda, T. Q. P.; Yumoto, N.; Kubo, T. *Biotechnol. Bioeng.* **2006**, *94* (3), 473−480.
(24) Taira, S.; Du, Y. Z.; Hiratsuka, Y.; Konishi, K.; Kubo, T.; Uyeda, T. Q. P.; Yumoto, N.; Kodaka, M. *Biotechnol. Bioeng.* **2006**, *95* (3), 533−538.
(25) Mihajlovic, G.; Brunet, N. M.; Trbovic, J.; Xiong, P.; von Molnar, S.; Chase, P. B. *Appl. Phys. Lett.* **2004**, *85* (6), 1060−1062.
(26) Huber, D. L.; Manginell, R. P.; Samara, M. A.; Kim, B. I.; Bunker, B. C. *Science* **2003**, *301* (5631), 352−4.
(27) Kawaguchi, K.; Ishiwata, S. *Cell Motil. Cytoskeleton* **2001**, *49* (1), 41−7.
(28) Kocer, A.; Walko, M.; Meijberg, W.; Feringa, B. L. *Science* **2005**, *309* (5735), 755−758.
(29) Zhu, Y.; Fujiwara, M. *Angew. Chem., Int. Ed.* **2007**, *46*, (13), 2241−2244.
(30) Martin, B. D.; Velea, L. M.; Soto, C. M.; Whitaker, C. M.; Gaber, B. P.; Ratna, B. *Nanotechnology* **2007**, *18* (5).
(31) Riveline, D.; Ott, A.; Julicher, F.; Winkelmann, D. A.; Cardoso, O.; Lacapere, J. J.; Magnusdottir, S.; Viovy, J. L.; Gorre-Talini, L.; Prost, J. *Eur. Biophys. J.* **1998**, *27* (4), 403−8.
(32) Böhm, K. J.; Stracke, R.; Mühlig, P.; Unger, E. *Nanotechnology* **2001**, *12*, 238−244.
(33) van den Heuvel, M. G. L.; De Graaff, M. P.; Dekker, C. *Science* **2006**, *312* (5775), 910−914.
(34) Kim, T.; Kao, M. T.; Hasselbrink, E. F.; Meyhofer, E. *Nano Lett.* **2007**, *7* (1), 211−217.
(35) Kim, T.; Kao, M. T.; Meyhofer, E.; Hasselbrink, E. F. *Nanotechnology* **2007**, *18* (2).
(36) Hutchins, B. M.; Platt, M.; Hancock, W. O.; Williams, M. E. *Small* **2007**, *3* (1), 126−131.
(37) Ionov, L.; Stamm, M.; Diez, S. *Nano Lett.* **2006**, *6* (9), 1982−1987.
(38) Hofstadter, D. R. *Gödel, Escher, Bach*; Vintage Books Edition; Random House: New York, 1980; p 777.
(39) Nitta, T.; Hess, H. *Nano Lett.* **2005**, *5* (7), 1337−1342.
(40) Du, Y. Z.; Hiratsuka, Y.; Taira, S.; Eguchi, M.; Uyeda, T. Q. P.; Yumoto, N.; Kodaka, M. *Chem. Commun.* **2005**, *40* (16), 2080−2082.
(41) Wikswo, J. P.; Prokop, A.; Baudenbacher, F.; Cliffel, D.; Csukas, B.; Velkovsky, M. *IEE Proc.: Nanobiotechnol.* **2006**, *153* (4), 81−101.
(42) Nakano, T.; Suda, T. *Appl. Soft Comput.* **2007**, *7* (3), 870−878.
(43) Helbing, D.; Deutsch, A.; Zerial, M.; Schulze, F.; Diez, S.; Breier, G.; Peters, K. *Ladenburger Discourse: From Bio-Inspired Logistics to Logistics-Inspired Bio-Nano-Engineering*, Ladenburg, Germany, April 3−4, 2007.
(44) Coy, D. L.; Wagenbach, M.; Howard, J. *J. Biol. Chem.* **1999**, *274*, (6), 3667−71.
(45) Bakker, B. M.; Mensonides, F. I. C.; Teusink, B.; van Hoek, P.; Michels, P. A. M.; Westerhoff, H. V. *Proc. Natl. Acad. Sci. U.S.A.* **2000**, *97* (5), 2087−2092.
(46) Howard, J.; Hunt, A. J.; Baek, S. *Methods Cell Biol.* **1993**, *39*, 137−47.
(47) Crank, J. *Mathematics of Diffusion*, 2nd ed.; Oxford University Press: Oxford, 1975.

NL072516N